Biochemical Pharmacology 213 (2023) 115633

Contents lists available at ScienceDirect

Biochemical Pharmacology

journal homepage: www.elsevier.com/locate/biochempharm

Neratinib is a TFEB and TFE3 activator that potentiates autophagy and unbalances energy metabolism in ERBB2+ breast cancer cells

Grazia Bellese [a], Erica Tagliatti [b,c], Maria Cristina Gagliani [a], Sara Santamaria [a], Pietro Arnaldi [a], Paola Falletta [d,e], Paola Rusmini [f], Michela Matteoli [b,g], Patrizio Castagnola [h,*,1], Katia Cortese [a,*,1]

[a] DIMES, Department of Experimental Medicine, Cellular Electron Microscopy Lab, Università di Genova, Genova, Italy
[b] IRCCS Humanitas Research Hospital, Laboratory of Pharmacology and Brain Pathology, via Manzoni 56, 20089 Rozzano, Milano, Italy
[c] Department of Clinical and Experimental Epilepsy, UCL Queen Square Institute of Neurology, University College London, London, United Kingdom
[d] Experimental Imaging Center, IRCCS Ospedale San Raffaele, Milan, Italy
[e] Vita-Salute San Raffaele University, Milan, Italy
[f] Dipartimento di Scienze Farmacologiche e Biomolecolari "Rodolfo Paoletti", Dipartimento di Eccellenza 2018-2027, Università degli Studi di Milano, Milan, Italy
[g] CNR Institute of Neuroscience, Milano, Italy
[h] IRCCS Ospedale Policlinico San Martino, Genova, Italy

ARTICLE INFO

Keywords:
Neratinib
Epidermal growth factor receptor 2
Tyrosine kinase inhibitors
Autophagy
Mitochondrial bioenergetics
TFEB

ABSTRACT

Neratinib (NE) is an irreversible pan-ERBB tyrosine kinase inhibitor used to treat breast cancers (BCa) with amplification of the ERBB2/HER2/Neu gene or overexpression of the ERBB2 receptor. However, the mechanisms behind this process are not fully understood. Here we investigated the effects of NE on critical cell survival processes in ERBB2^{+} cancer cells. By kinome array analysis, we showed that NE time-dependently inhibited the phosphorylation of two distinct sets of kinases. The first set, including ERBB2 downstream signaling kinases such as ERK1/2, ATK, and AKT substrates, showed inhibition after 2 h of NE treatment. The second set, which comprised kinases involved in DNA damage response, displayed inhibition after 72 h. Flow cytometry analyses showed that NE induced G0/G1 cell cycle arrest and early apoptosis. By immunoblot, light and electron microscopy, we revealed that NE also transiently induced autophagy, mediated by increased expression levels and nuclear localization of TFEB and TFE3. Altered TFEB/TFE3 expression was accompanied by dysregulation of mitochondrial energy metabolism and dynamics, leading to a decrease in ATP production, glycolytic activity, and a transient downregulation of fission proteins. Increased TFEB and TFE3 expression was also observed in

Abbreviations: AKT, Protein kinase B; ANOVA, Analysis of variance; ATP, Adenosine triphosphate; AV, autophagic vacuole; BCa, Breast cancers; BSA, Bovine serum albumin; CHK2, Checkpoint kinase 2; CREB, cAMP response element-binding protein; DAPI, 4′,6-diamidino-2-phenylindole; CLEAR, Coordinated Lysosomal Expression and Regulation; DDR, DNA damage response; DMEM, Dulbecco's modified Eagle medium; DRP-1, Dynamin-related protein 1; DPP, differentially phosphorylated proteins; DXd, Deruxtecan; ECL, Enhanced chemiluminescent; ECAR, Extracellular acidification rate; EM, Electron microscopy; ERBB, Epidermal growth factor receptor family of tyrosine kinase receptors; ERBB1, Epidermal growth factor receptor 1; ERBB2/HER2/Neu, erythroblastic leukemia viral oncogene homolog 2 gene and receptor associated with breast cancer; ERBB2, Epidermal Growth Factor Receptor 2; ERK1/2, Extracellular signal-regulated kinase; ExteNET, Extended Adjuvant Treatment of Early-Stage Breast Cancer with Neratinib; FCCP, Carbonyl cyanide-4-(trifluoromethoxy)phenylhydrazone; G2/M, G2-phase/mitosis; GAPDH, Glyceraldehyde-3-Phosphate Dehydrogenase; GSK, Glycogen synthase kinase; HSP90, Heat shock protein 90; hr DNA-FCM, High-resolution DNA flow cytometry; IC50, Half maximal inhibitory concentration; IF, Immunofluorescence; LAMP-1, Lysosomal-associated Membrane Protein 1; MAP1LC3B, Microtubule-Associated Protein 1 Light Chain 3 Beta; MFN-1, Mitofusin 1; MFF, Mitochondrial Fission Factor; Mit, mitochondrion; mTOR, Mammalian target of rapamycin; MQC, Mitochondrial quality control; MR, Magic Red; NE, Neratinib; NH_4Cl, Ammonium chloride; OCR, Mitochondrial oxygen consumption rate; OD520, Optical density at 520 nm; PFA, Paraformaldehyde; PBS, Phosphate-buffered saline; PARP1, Poly(ADP-ribose) polymerase 1; pATK, Phosphorylated protein kinase B; pATK S473, Phosphorylated protein kinase B at serine 473; pERK, Phosphorylated extracellular signal-regulated kinase; p53, Tumor protein p53; PRAS40, Proline-rich Akt substrate of 40 kDa; p62/SQSTM1, p62/Sequestosome 1; Ph, phagofore membranes; RSK, Ribosomal S6 kinase; TFEB, Transcription factor EB; TFE3, Transcription factor E3; TKIs, Tyrosine kinase inhibitors; TSLs, Terminal storage lysosomes; TZ, Trastuzumab; T-DXd, Trastuzumab deruxtecan; WNK1, Lysine Deficient Protein Kinase 1.

* Corresponding authors.
E-mail addresses: patrizio.castagnola@hsanmartino.it (P. Castagnola), cortesek@unige.it (K. Cortese).
[1] These authors contributed equally.

https://doi.org/10.1016/j.bcp.2023.115633
Received 25 March 2023; Received in revised form 17 May 2023; Accepted 26 May 2023
Available online 1 June 2023

ERBB2-/ERBB1 + BCa cells, supporting that NE may act through other ERBB family members and/or other kinases. Overall, this study highlights NE as a potent activator of TFEB and TFE3, leading to the suppression of cancer cell survival through autophagy induction, cell cycle arrest, apoptosis, mitochondrial dysfunction and inhibition of DNA damage response.

1. Introduction

ERBB2 is a member of the epidermal growth factor receptor (ERBB1) family and chaperoned at the plasma membrane by the heat shock protein 90 (HSP90) [1]. Unlike other ERBB members, ERBB2 has no soluble ligands. Upon activation, ERBB receptors homodimerize or heterodimerize, and ERBB2 is the preferred dimerization partner, constituting a potent signaling module [2]. In normal epithelial cells, dimerized ERBB receptors activate the PI3K/AKT/mTOR and MAPK/ERK-dependent pathways that govern cell survival, autophagy, and cell proliferation [3]. The dysregulation of the ERBB signaling network, endocytic and autophagy abnormalities, as well as metabolic reprogramming are emerging common features of many cancers [4], including breast cancer (BCa), contributing to tumor progression, and therapy resistance [5–9]. In BCa, the overexpression of human epidermal growth factor receptor 2 (ERBB2/HER2) caused by gene amplification accounts for approximately 20%–30% of cases. This molecular subtype, now defined as ERBB2/HER2-enriched or HER2-E, is associated with relapse, higher risk of metastases, and poor prognosis [1].

The development of targeted therapies aimed at ERBB2 has dramatically improved the prognosis of patients with ERBB2$^+$ BCa. Trastuzumab (TZ, Herceptin®) represents the gold standard for ERBB2 + BCa therapy [5,6], whereas the recently FDA-approved TZ-deruxtecan (TZ-DXd, Enhertu®) is under intense clinical investigation for both ERBB2-E and ERBB2-low BC subtypes [10,11]. Tyrosine kinase inhibitors (TKIs) such as lapatinib and neratinib (NE, HKI-272), in association with therapeutic antibodies and, less frequently, HSP90 inhibitors [3,12], are also intensively studied at both the preclinical and clinical levels. Neratinib (NE) is an irreversible pan-ERBB tyrosine kinase inhibitor approved in 2017 for extended adjuvant treatment of early-stage ERBB2/HER2 positive BCa based on the ExteNET trial [13,14] that causes survival inhibition of ERBB2$^+$ cancer cells and is currently approved only for ERBB2$^+$ BCa. In BCa, NE is active in ERBB2$^+$-amplified cancer cell lines at very low nanomolar IC_{50} values and is metabolized in lysosomes [9,15–19]. However, the mechanisms behind survival inhibition are not yet fully understood [13,14]. As NE targets multiple tyrosine and serine/threonine kinases beyond the ERBB family, this raised the attention on the repurposing of NE for lung, colorectal, and bladder cancers, leukemia, diabetes, inflammatory diseases, and neurodegenerative disorders [20,9,15–19] Therefore, a better understanding of its mechanism/s of action is warranted.

Autophagy is a catabolic process that clear damaged intracellular components and recycles metabolites. This process plays a crucial role in meeting metabolic demands during nutrient deprivation, hypoxia, genotoxic stress, and low levels of growth factors. However, the role of autophagy in tumorigenesis is paradoxical and dependent on the stage of tumor development. At an early stage, autophagy acts as a tumor suppressor by degrading potentially oncogenic molecules. On the other hand, in the advanced stages of tumor development, autophagy promotes the survival of cancer cells by mitigating stress in the microenvironment [21]. TKIs can induce two different cellular processes: cytoprotective autophagy [22], which is part responsible for drug resistance and cancer cell survival, and cell death by apoptosis. However, in some cases, TKIs can induce autophagy in a way that actually facilitates cancer cell's death. For example, Lapatinib is an oral dual TKI that can induce autophagy, which in turn help to trigger apoptosis in ERBB2-positive BCa [23]. Conversely, ablation of autophagy genes in ERBB2 + mouse models can prevent early tumorigenesis by decreasing ERBB2 expression and trafficking to lysosomes, while increasing its release in exosomes [24].

In this study, we investigated the effects of NE on the transcription factors TFEB and TFE3, which regulate critical processes such as autophagy and mitochondrial homeostasis that promote cancer cell survival. Our data show that NE time-dependently inhibited ERBB2 and different sets of kinases involved in cell survival and DDR in ERBB2 + breast cancer cells. In addition, we reported for the first time that NE strongly enhanced total TFEB/TFE3 expression and its nuclear localization, potentiating autophagy. Notably, NE modulates TFEB protein levels in ERBB1+/ERBB2- BCa cells, supporting that NE acts on TFEB through ERBB receptors and not exclusively through ERBB2. Finally, mitochondria bioenergetics, ultrastructural morphology, and dynamics were also strongly affected as a possible consequence of NE-induced TFEB modulation. Collectively, these findings broaden the understanding of NE biology on ERBB2 + BCa cells and identify NE as a potent TFEB activator in ERBB2 + BCa and ERBB2- BCa cells.

2. Materials and methods

2.1. Cell culture and treatments

ERBB2$^+$ overexpressing SKBR-3, BT474, and triple negative ERBB2-/ERBB1 + MDA-MB-231 cells were obtained from Banca Biologica and Cell Factory in IRCCS Ospedale Policlinico San Martino belonging to the European Culture Collection's Organization (Porton Down, Wiltshire, UK). SKBR-3, BT474 and MDA-MB-231 were cultured in complete medium (DMEM high glucose supplemented with 10% heat-inactivated fetal bovine serum, 1% glutamine, penicillin and streptomycin (Euroclone S.p.A., Milan, Italy). Neratinib (Nerlynx, Puma Biotechnology, Inc. Los Angeles, CA) was purchased from Sigma-Aldrich (CAS Number: 698387–09-6, St. Louis, MI, USA) and dissolved in Dimethyl sulfoxide (DMSO, CAS Number 67–68-5, Sigma-Aldrich St. Louis, MI, USA) at 50 μM.

We performed concentration-dependent survival analysis by MTT assay and assessed that 6 nM and 4.5 nM NE were capable to inhibit after 72 h of treatment SKBR-3 and BT474 cell survival at 50% (IC50) compared to control cultures treated with 0.012% DMSO (data not shown), respectively. These IC50 NE concentrations were used for all subsequent experiments with SKBR-3 and BT474. For ERBB2-/ERBB1 + MDA-MB-231 BCa cells, we used the highest concentration (6 nM) of NE used to evaluate TFEB and/or TFE3 induction in all the experiments.

2.2. Antibodies and reagents

Antibodies: mouse monoclonal anti-ErbB2 (neu Ab-20 (L87 + 2ERB19); (Thermo Scientific, Waltham, MA, USA) and rabbit polyclonal Phospho-ERBB2 (Y1248) (#2247, Cell Signaling, Danvers, MA, USA) were used for Western blot analysis, and mouse anti-ErbB2 9G6 (Santa Cruz Biotechnology, Dallas, TX, USA) was used for EM studies and fluorescence microscopy. Mouse monoclonal anti-LAMP1 (H4A3) (Developmental Studies Hybridoma Bank, University of Iowa, Iowa City, IA) was used for immunofluorescence. Antibodies to pan-AKT (clone 40D4, #2920) was purchased from Cell Signaling technology, Danvers, MA, USA, p-AKT1/2/3 (ser 473, sc-7985-R), and ERK1/2 (MK1, sc-135900) were purchased from Santa Cruz Biotechnology, Dallas, TX, USA. pERK1/2 (#9101) from Cell Signaling technology, Danvers, MA, USA. Rabbit monoclonal LAMP-1 (D2D11) from Cell Signaling technology Danvers, MA, USA, anti-SQSTM1/p62 (Abnova, Taipei, Taiwan, H00008878-M01); anti-LC3A/B (Novus Biological, Englewood, CO,

USA, NB100-2220); anti-TFEB (Bethyl Laboratories, Montgomery, TX, USA, A303-673A), rabbit polyclonal anti-TFE3 (1:2,000, Sigma-Aldrich, St. Louis, MI, USA, #HPA023881), anti-GAPDH (FL-335; Santa-Cruz Biotechnology, Dallas, TX, USA, sc-25778; 1:3,000), anti-Lamin B1 (ab16048 Abcam, Cambridge, UK), anti-vinculin (V9131, Sigma-Aldrich, St. Louis, MI, USA), monoclonal anti-ß actin (Invitrogen, Waltham, MO, USA, 15G5A11/E2). Mitochondria dynamics Antibody sampler kit II (#74792) was purchased from Cell Signaling technology, Danvers, MA, USA.

2.3. Flow cytometry (FCM) analysis

Both adherent and floating cells were collected after 72 h of 6 nM NE treatment and centrifuged at 980g for 5 min. DNA content in cell nuclei was measured by staining with DAPI and high-resolution DNA flow cytometry (hr DNA-FCM) using a Sysmex-Partec CyFlow ML flow cytometer (Sysmex-Partec GmbH, Görlitz, Germany). Cell cycle phases were determined by using the Partec CyFlow software. Apoptotic and necrotic cells were evaluated by using the Vybrant Apoptosis Assay Kit purchased from Thermo Fisher Scientific, Waltham, MA, USA, with a minor procedure modification as we used the nuclear staining fluorochrome sytox blue instead of the sytox green. Cells were then analyzed using a Beckman Coulter Cyan ADP flow cytometer (Beckman Coulter Life Sciences, Brea, CA, USA). An ANOVA with Tukey's post-test was performed for both cell cycle and apoptosis assays to assess statistical significance.

2.4. Human Phospho-Kinase array

To simultaneously detect the relative site-specific phosphorylation of 37 kinase phosphorylation sites and 2 related total proteins we used the human phospho-kinase dot blot array (ARY003C; R&D Systems, Inc., Minneapolis, MN, USA). An equal amount of cell lysate (500 μg) from SKBR-3 cell line treated with NE at a 6 nM or DMSO for 2 h and 72 h was used for these experiments. The enhanced chemiluminescent (ECL) signal was visualized using a Uvitec Cambridge gel doc system (UVITEC Cambridge Ltd. Innovation Centre, Cambridge, CB4 0FZ UK) and NineAlliance software (Cambridge, UK). All arrays of one experiment were exposed simultaneously. The Uvitec NineAlliance software (Cambridge Ltd. Innovation Centre, Cambridge, CB4 0FZ UK) was used to quantify phosphorylation and expression levels of the proteins. The pixel density of the background signal was subtracted from the average of measured signal of a pair of dots for each protein on the array. The phosphorylated level of each protein in NE-treated group was determined by normalizing it to the pixel density value in the respective DMSO control group. An arbitrary 50% cut-off was applied to detect significant phospho-kinase or protein level modulations.

2.5. Immunofluorescence and microscopy analyses

For immunofluorescence analysis, SKBR-3 cells were treated for 2 and 72 h with 6 nM NE (single dose treatment), fixed in 3% paraformaldehyde (PFA) in phosphate-buffered saline (PBS) pH 7.4 for 20 min and then quenched with 30 mM NH_4Cl. Cell permeabilization was performed with 0.2% saponin in 0.1% BSA for LAMP1 (H4A3, Developmental studies Hybridoma Bank, Iowa City, IA) staining. Cells were washed 3 times with PBS and incubated with secondary antibodies conjugated to Alexa Fluor 546 or 488 (Thermofisher Scientific, Waltham, MA, USA) for 20 min at room temperature. Coverslips were washed 3 times in phosphate buffered saline (PBS) and mounted using an anti-fading mounting media (Prolong Gold, Thermofisher Scientific, Waltham, MA, USA). Image acquisition was performed using an Olympus IX70 (Olympus Corporation, Tokyo, Japan) wide field microscope equipped with Hamamatsu camera Orca-Flash 4.0 V3/LT+ (Hamamatsu, Japan). Images were analyzed by Huygens Professional suite using the object analyzer tool (Scientific Volume Imaging B.V. VB Hilversum, The Netherlands).

2.5.1. Measurement of lysosomal activity by Magic Red cathepsin B assay

For lysosomal activity assay, a Magic Red live staining (#937, ImmunoChemistry Technologies, LLC (ICT), Bloomington, Minnesota, USA) was performed onto bottom glass petri dishes (3 cm) by dilution into culture medium to 10 μg/ml and incubated for 2 h at 37° C as described by the manufacturer. Microscopy images were automatically analyzed by Huygens Professional suite (Scientific Volume Imaging B.V. VB Hilversum, The Netherlands) using the object analyzer tool. The results were plotted as histograms (mean ± SEM), N = 3 independent experiments.

2.6. Transmission electron microscopy

For the analysis of the uptake of 5 nm BSA-gold, DMSO and NE treated SKBR-3 cells were incubated with BSA-gold (OD520 = 5) (Cell Microscopy Core, Utrecht, The Netherlands) for 2 h 37° C and processed as described. SKBR-3 cells were washed out twice in 0.1 M cacodylate buffer (Sigma-Aldrich, St. Louis, MI, USA) and fixed in 0.1 M cacodylate buffer containing 2.5% glutaraldehyde (Electron Microscopy Science, Hatfield, PA, USA) or 1 h at room temperature. The cells were postfixed in 1% osmium tetroxide for 10 min (VWR International, PA, USA) and 1% aqueous uranyl acetate (SERVA Electrophoresis GmbH, Heidelberg Germany) for 1 h. Subsequently, samples were dehydrated through a graded ethanol series (Merck, Darmstadt, Germany) and flat embedded in epoxy resin (Poly-Bed; Polysciences, Inc., Warrington, PA) for 24 h at 60 °C. Ultrathin sections (50 nm) were cut parallel to the cell monolayer and counterstained with 5% uranyl acetate in 50% ethanol. Electron micrographs were acquired using a Hitachi 7800 120Kv electron microscope (Hitachi, Tokyo, Japan) equipped with a Megaview G3 digital camera and Radius software (EMSIS, Muenster, Germany). For EM morphometry, we classified lysosomes as single-membrane round organelle with electron dense appearance and both membranaceous and amorphous content positive for 5 nm BSA gold. BSA- positive electron lucent multivesicular endosomes (>10 intraluminal vesicles) and early endosomes (<10 intraluminal vesicles) were not considered for morphometry. 10 whole cells were scored for lysosomes and counted (N = 3 independent experiments). To perform mitochondria morphometry, ten whole cells were scored for mitochondria and measured with line tool of Radius 2.0 software (N = 3 independent experiments).

2.7. Immunoblot analysis

To perform nuclear-cytoplasmic TFEB localization by immunoblot, SKBR-3 were seeded at 180,000 cell/well in 6-well plates, treated as explained in the text and incubated for 2 h and 72 h. Cells were collected and centrifuged at 375 g for 5 min. at 4 °C. Pellets were lysed in Triton X-100 lysis buffer (50 mM Tris-HCl, pH 7.5, 0.5% Triton X-100 (Sigma-Aldrich, St. Louis, USA), 137.5 mM NaCl, 10% glycerol (G5516, Sigma-Aldrich, St. Louis, USA), 5 mM ethylenediaminetetraacetic acid, Sigma-Aldrich, St. Louis, USA), sodium orthovanadate and PhosStop (Roche, Roche Holding AG, Basel Switzerland) and nuclear-cytoplasmic fractions were isolated as described previously [25].

For western blotting, SKBR-3, BT474 and MDA-MB-231 cells were lysed using lysis buffer (Hepes pH 7.4 20 mM, NaCl 150 mM, 10% Glycerol, 1% Triton X-100) supplemented with protease inhibitors cocktail Complete (Roche Applied Science, Penzberg, Germany) and sodium orthovanadate and PhosStop (Roche, Roche Holding AG, Basel Switzerland). Proteins were resolved on SDS-polyacrylamide gel electrophoresis (Thermo Fisher Scientific Inc. Waltham, MA, USA) and blotted on nitrocellulose (GE Healthcare Life Science, Amersham Buckinghamshire, UK) or PVDF (Merck Millipore, Darmstadt, Germany) membranes. Detection was performed using a ECL Detection Reagent (BIORAD, Hercules, CA, USA) according to manufacturer's protocol. ECL signals were detected, recorded, and measured with the Uvitec

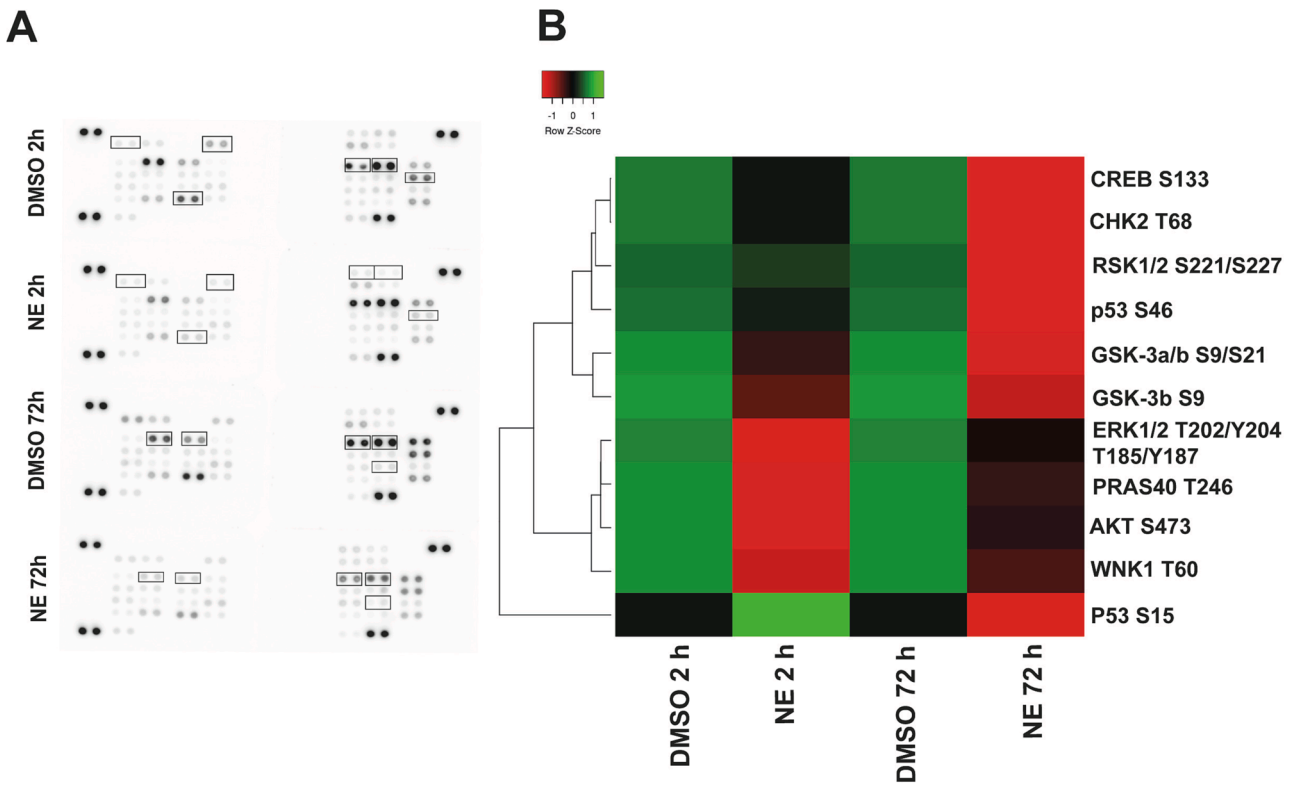

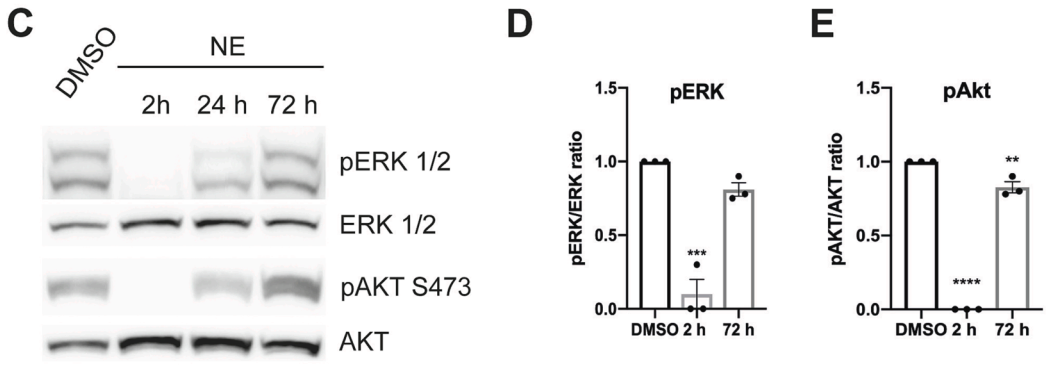

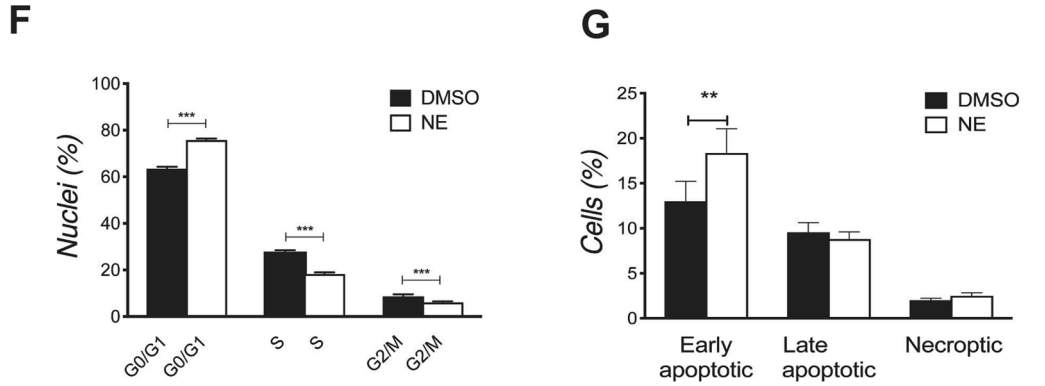

(caption on next page)

Fig. 1. *Time-dependent modulation of protein phosphorylation by NE.* (A) Phospho-kinase array immunoblot of SKBR-3 cells treated with 6 nM NE or DMSO, used as solvent control, for 2 h and 72 h. A cut-off of 50% of signal intensity modulation was applied to identify differentially phosphorylated proteins (DPP), which are indicated by boxes. (B) An unsupervised hierarchical-clustered heatmap of DPP was generated. The extent of phosphorylation modulation for each protein is represented by the color scheme in which red and green indicate downregulation and upregulation, respectively. (C) SKBR-3 cell lysates treated with NE for 2, 24 and 72 h were subjected to immunoblot analysis with antibodies to pERK1/2 and p-AKT ser473. Total ERK and AKT were used as loading control. (D-E) Quantification of band intensity of pERK and pAKT relative to total ERK and AKT. Values are normalized to DMSO. Error bar = SEM. Significance was determined using one-way ANOVA from n = 3 independent experiments. (F) NE arrests cell cycle in G0/G1 in SKBR-3 cells. A hr DNA-FCM analysis of DAPI-stained nuclei of cells cultured for 72 h with control medium (DMSO) and 6 nM NE supplemented medium. Both floating and adherent cells were collected for the analysis. Mean values and standard deviation (indicated as vertical bars) from four independent replicates (n = 4) are shown. (G). NE induces early apoptosis in SKBR-3 cells. The percentage of early and late apoptotic cells, and necrotic cells after 72 h of exposure to NE or DMSO is shown. Mean values and SD (indicated as vertical bars) (n = 3) are shown. Statistical significance: $P < 0.01$ (**), $P < 0.001$ (***), $P < 0.0001$ (***).

Cambridge gel doc system and software (UVITEC Cambridge Ltd. Innovation Centre, Cambridge, Cambridge, UK). ERBB2 was detected with anti-ERBB2 N-terminal (Ab-20, Thermo Scientific Inc. Waltham, MA, USA), anti-ERBB2 C-terminal (C-18, sc-284 Santa Cruz Biotechnology, Santa Cruz, CA, USA) antibodies. Anti-vinculin antibody (V9131, Sigma-Aldrich, St. Louis, MI, USA) was used as loading control.

2.8. Seahorse analysis

Oxygen consumption rate (OCR) and extracellular acidification rate (ECAR) under Neratinib 2 h and 72 h were determined using a Seahorse XF96 Extracellular Flux Analyzer (Agilent Technologies, Santa Clara, California, USA) and the Seahorse XF Cell Mito Stress test Kit (#103015–100, Agilent Technologies, Santa Clara, California, USA) following the manufactures' instructions guidelines. Ninety-six hours prior to the assay, 6,200 SKBR-3 cells/well were seeded in XF96 plates. OCR and ECAR were monitored according to the manufacturer's instructions. Briefly, the day of the experiment, SKBR-3 cells were treated with Neratinib (6 nM) or corresponding volume of DMSO for 2hr. After this treatment, the medium was replaced with Agilent Seahorse DMEM, pH 7.4, enriched with glucose (10 mM), glutamine (2 mM) and pyruvate (1 mM). A baseline recording followed by sequential injection of the ATP-synthase inhibitor oligomycin A (1.5 μM), the ATP synthesis uncoupler carbonyl cyanide-4-trifluoromethoxyphenylhydrazone (FCCP) (2 μM) and the Complex I and III inhibitor mix Rotenone/Antimycin A (0.5 μM) was recorded in 10-replicates/conditions. Three measurements of OCR and ECAR at each experimental point were taken. Three independent experiments were performed. Data are expressed as % of the baseline.

2.9. Statistical analysis

All in vitro experiments were repeated at least three times. The data were analyzed using GraphPad Prism 8 (GraphPad Software, San Diego, CA, USA). Statistical differences in the average among two or more groups were compared using Student *t* test or Analysis of Variance (ANOVA), *p < 0.05, **p < 0.01, ***p < 0.001, ****p < 0.0001.

3. Results

3.1. NE time-dependently modulates different sets of phosphokinases

NE is a pan-ERBB approved only to treat ERBB2 + BCa. However, recent work showed that NE exerts inhibitory activity on multiple kinases other than ERBB receptors [26]. Our starting point was to investigate the inhibitory activity of NE in our ERBB2-overexpressing cell model SKBR-3 cells. We performed molecular analysis of cell lysates treated with NE or DMSO used as a control for 2 h and 72 h using a commercially available phospho-kinase Array. NE time-dependently inhibited the phosphorylation of two distinct sets of kinases (Fig. 1 A, B). The first set was suppressed at 2 h of treatment and included some ERBB2 downstream signaling kinases such as ERK1/2, ATK S473, and AKT substrates (PRAS40 and WNK1). The immunoblot analysis focused on the ERBB2-dependent signaling pathways pATK S473/AKT and pERK/ERK1/2 and confirmed that these kinases were significantly suppressed at 2 h of treatment and reactivated at 72 h (Fig. 1 C-D-E). By contrast, at 72 h of NE, while the first set was no longer affected, a second set of kinases and kinase substrates involved in DDR were strongly inhibited (CREB S133, CHK2 T68, RSK ½ S221/S227, p53 S46, S15, GSK 3a/b S9/S21, and GSK 3b S9). In agreement with these results, we found by hr DNA-FCM analysis that NE increased the percentage of cells in the G0/G1 phases compared with control cultures at 72 h. This arrest in G0/G1 was accompanied by a significant reduction of the percentage of cells in the S and G2/M phases (Fig. 1 F). As a downregulation of DDR response kinases might indicate the activation of apoptosis, an apoptosis assay was performed by FCM. The number of early apoptotic cells in NE-treated SKBR-3 was significantly higher than that of control cultures (Fig. 1G).

ERBB2 phosphorylation (Y1248) and total ERBB2 expression levels were further assessed by cell fractionation assay and immunoblot analysis, which confirmed that NE transiently and significantly switched off ERBB2 Y1248 phosphorylation without reducing ERBB2 levels, as revealed by an antibody recognizing the N- terminal domain of ERBB2. (Fig. 2 A, quantification in B-C). These results suggest that in our cell model, NE sequentially switches on, or off ERBB2 signaling and multiple kinases involved in both cell survival and, as a late event, DDR.

3.2. NE transiently enhances TFEB and TFE3 expression promoting autophagy

Autophagy is coordinated by TFEB and TFE3, two master transcriptional factors that regulate the transcription of a gene network controlling autophagosome formation, lysosome biogenesis, and MQC [27,28]. As inactive phosphorylated TFEB is located predominantly in the cytoplasm and active, dephosphorylated TFEB is found in the nucleus, we investigated the subcellular localization of TFEB by cell fractionation assays under NE treatment in SKBR-3 cells. As presented in Fig. 2 D and 2H, NE significantly increased both the cytoplasmic and nuclear levels of TFEB and TFE3 at 2 h and 24 h of treatment compared with controls. By contrast, at 72 h of NE treatment, the levels of TFEB, and TFE3 returned similar to those of controls (Fig. 2 E, F, I, J). This result suggests that NE induced a potent but transient expression of TFEB/TFE3 and its nuclear localization. Interestingly, in ERBB2 + BT474 cells, which express negligible levels of TFEB, NE still modulated TFE3 expression (Fig. 2 M, quantification showed in Fig. 2 N-P). However, NE drives a significant induction of TFEB also in MDA-MB-231 cells, an ERBB1/EGFR overexpressing triple-negative BCa cell line, indicating that TFEB induction by NE is not specifically related to ERBB2 inhibition (Fig. 2 Q and R). These results suggest a cell-context dependency of NE-induced TFEB and/or TFE3 modulation. Then, we assessed autophagy and lysosomal marker levels by immunoblot analysis in SKBR3 exposed to NE for 2 and 72 h at 37 °C. Microtubule-associated protein light chain 3 beta (MAP1LC3B, hereafter referred to as LC3) and the cargo protein SQSTM1/p62 were used as markers of autophagic flux, while LAMP-1 was used to monitor lysosomes. As shown in Fig. 2H, NE significantly but transiently decreased both LC3-II and SQSTM1/p62 levels after 2 h of treatment, whereas at 72 h, both proteins returned to nearly control levels (Fig. 2 K-L). Instead, the levels

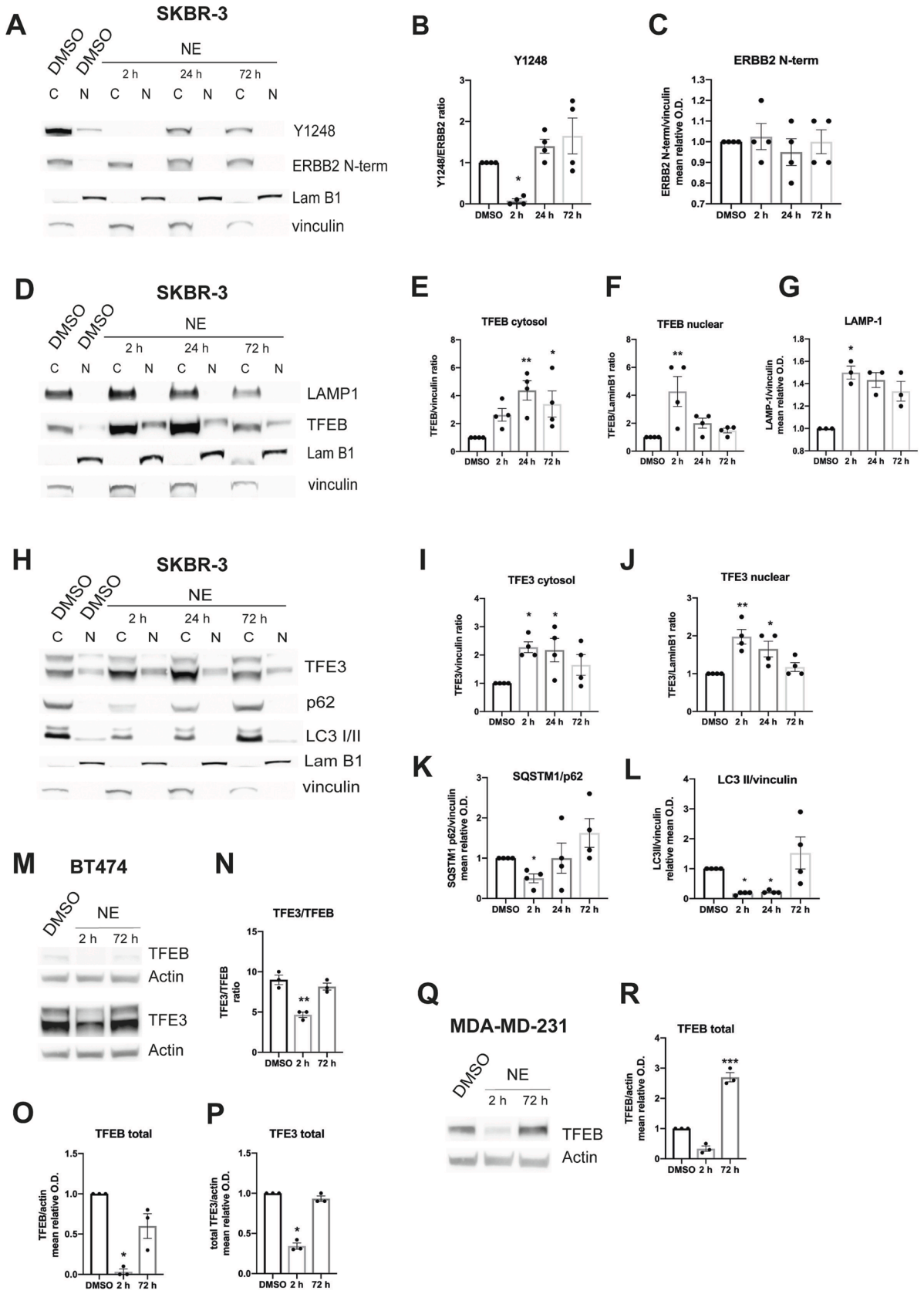

(caption on next page)

Fig. 2. *NE transiently induces TFEB-mediated autophagy.* (A, D, H) Representative western blotting (WB) analysis of cytoplasmic (C) and nuclear (N) extracts of SKBR-3 overexpressing ERBB2 at several time points of treatment with NE or DMSO. Vinculin was used as loading control of the cytoplasmic fraction. Lamina B1 (Lam B1) was used as loading control of the nuclear fraction. (A) To visualize ERBB2, an anti-ERBB2 antibody was used to detect the N-terminal of ERBB2. Anti-phospho Y1248 was used to detect ERBB2 phosphorylation status upon NE. (B, C) Quantification of WB shown in Fig. 2 A. Each bar graph represents the mean relative optical density quantification of phospho ERBB2 (Y1248) (B) and total ERBB2 (N-terminal domain) (C) signals. Total ERBB2 was used as control for Y1248. Values are normalized to DMSO. Error bar = SEM. Significance was determined using one-way ANOVA from n = 4 independent experiments. (D) To visualize the lysosomal protein LAMP-1, the transcription factors transcription factor EB (TFEB) anti-LAMP1 antibodies were used. (E-G) Quantification of WB shown in Fig. 2 D. (E) Each bar graph represents the mean relative optical density quantification of cytoplasmic fraction of TFEB signals. (F) The bar graph represents mean relative optical density quantification of nuclear TFEB signals. (G) The bar graph represents mean relative optical density quantification of LAMP-1 signals. Values are normalized to DMSO. Error bar = SEM. Significance was determined using one-way ANOVA from n = 4 independent experiments. (H) To visualize the transcription factor TFE3, the p62 and the LC3 proteins, anti-TFE3, anti-p62 and anti-LC3 antibodies were used. (I-L) Quantification of WB shown in Fig. 2 H. (I) The bar graph represents the mean relative optical density quantification of cytoplasmic fraction of TFE3 signals. (J) The bar graph represents mean relative optical density quantification of nuclear TFE3 signals. (K) The bar graph represents the mean relative optical density quantification of SQSTM1/p62 signals. (L) The bar graph represents the mean relative optical density quantification of LC3 I/II signals (lower lane considered). (M) Immunoblot analysis of total TFEB and TFE3 expression levels in ERBB2 + BT474 cell line after 2 and 72 h of 4.5 nM NE treatment. To visualize the transcription factor TFEB and TFE3, anti-TFEB and TFE3 antibodies were used. Actin was used as loading control. (N-P) Quantification of WB shown in Fig. 2 M. (N) The bar graph represents the TFE3/TFEB signal ratio in BT474 cells. (O) The bar graph represents mean relative optical density quantification of total TFEB signal. (P) The bar graph represents mean relative optical density quantification of total TFE3 signal. Values are normalized to DMSO. Error bar = SEM. Significance was determined using one-way ANOVA from n = 3 independent experiments. (Q) Immunoblot analysis of TFEB expression in MDA-MB-231 triple negative BCa cell line after 2 and 72 h of 6 nM NE treatment. Actin was used as loading control. (R) Quantification of WB shown in Fig. 2 Q. The bar graph represents mean relative optical density quantification of total TFEB signal. Values are normalized to DMSO. Error bars = SEM. Significance was determined using one-way ANOVA from n = 3 independent experiments. Statistical significance: *p < 0.05, P < 0.01 (**), P < 0.001 (***).

of LAMP-1 followed the same trend of TFEB, significantly increasing after 2 h of NE and returning similar to DMSO after 72 h (Fig. 2 G). Although the strong reduction of LC3-II levels might indicate autophagy inhibition, the concomitant decrease of SQSTM1/p62 and the increment of nuclear TFEB/TFE3 and LAMP-1 levels suggest instead an intense autophagic flux that consumes both LC3-II and p62. Collectively, these results indicate that at early stages of treatment, NE potently activates autophagy through TFEB and TFE3, whereas the process is turned off after 72 h.

3.3. NE increases lysosomal reformation and does not impair their degradative activity

To better characterize autophagic flux under NE, we performed immunofluorescence analysis to evaluate lysosomes, the terminal organelles of autophagy in SKBR-3cells. Specifically, lysosomal activity was assessed by immunofluorescence using the Magic Red (MR) probe (cathepsin B assay), whereas the lysosomal number, and size were measured by LAMP-1 immunostaining in SKBR3cells. While at 2 h of NE treatment, the number of LAMP-1 positive lysosomes significantly increased but the size was reduced, at 72 h no changes were observed, compared with controls (Fig. 3 A, B). Concerning lysosomal activity, no significant differences compared to controls were observed in MR fluorescence at both time points (Fig. 3 C, D). These data suggest that a fraction of LAMP-1 positive lysosomes in NE-treated cells might be newly formed lysosomes (Fig. 3 D). Terminal storage lysosomes (TSLs) are not acidic, inactive lysosomes reformed from endolysosomes/autolysosomes to maintain the dynamic equilibrium of the late endocytic pathway [29]. An ultrastructural examination of the endolysosomal compartment of SKBR-3cells, visualized using 5 nm gold-conjugated BSA as an endocytic tracer, revealed the presence of both endolysosomes/autolysosomes and *bona fide* small-sized electron-dense TSL, which were more abundant in NE-treated cells (Fig. 4 A). TSLs appeared as small (200–300 nm) and BSA-gold positive in NE-treated cells (Fig. 4 A, black arrows). Accordingly, EM morphometric analysis confirmed a significant increase in the number of total lysosomes (endolysosomes and terminal lysosomes) after 2 h of NE treatment. Contrastingly, no statistically significant differences in lysosomal number were observed at 72 h (Fig. 4 B). In NE-treated cells, damaged mitochondria are engulfed by autophagic membranes, suggestive of an imbalance in mitochondrial function and mitophagy (Fig. 4 C).

3.4. NE unbalances energy metabolisms and mitochondrial dynamics

To address whether the mitophagy-related figures observed at the EM level upon NE treatment reflected an impairment of mitochondrial function, we examined the mitochondrial oxygen consumption rate (OCR) using a Seahorse Extracellular Flux Analyzer. This tool allowed real-time and live cell analyses in SKBR-3 cells treated for 2 and 72 h (Fig. 5). In addition, the glycolytic activity of these cells was indirectly determined by the extracellular acidification rate (ECAR), which measured lactic acid production as a glycolytic activity indicator. Both OCR and ECAR were already and significantly inhibited in NE-treated cells for 2 h (Fig. 5 A, B). Indeed, basal respiration in NE-treated cells was strongly reduced compared with that in controls; Fig. 5 C). During the mitochondrial stress test, cells treated with NE for 2 h showed a significant reduction of ATP-coupled respiration after the injection of oligomycin (Fig. 5 E), and of the maximal respiration after the injection of FCCP compared with controls (Fig. 5 G). In addition, we observed a significant reduction of proton leak (Fig. 5 F), while no effects were observed in the spare (reserve) respiratory capacity (Fig. 5 H). Finally, we observed a significant inhibition of non-mitochondrial respiration (Fig. 5 I). These data clearly demonstrated that NE impaired mitochondrial function. A longer treatment time (72 h), NE dramatically depressed overall OCR and ECAR, suggesting greatly reduced cell viability (Fig. 5 J, K). As MQC is controlled by TFEB/TFE3 [28] and NE acts as a TFEB agonist in SKBR-3 cells, a detailed microscopic analysis was performed to investigate mitochondrial structural rearrangements. We characterized mitochondrial morphology and size with single-organelle resolution (Fig. 6 A, B). High-resolution images of SKBR-3 cells revealed that the mitochondria were primarily fused with more elongated shapes in 2 h NE-treated cells, which was distinct from the network morphology observed in control cells. In contrast, after 72 h of NE treatment the mitochondrial network appeared more fragmented (Fig. 6 A). The diameter (long axis) of > 200 mitochondria was measured in NE-treated cells, correlated with the controls, and showed a significant increase in size after 2 h, while significant reduced size and fragmentation were observed after 72 h. Moreover, the mitochondria of the untreated cells contained well-organized cristae with predominantly transverse orientation with respect to the long axis of the organelle (Fig. 6 A, white box, enlargement in the lower left panel). By contrast, the mitochondria of 2–72 h NE-treated cells contained more electron-dense matrix and poorly distinct cristae (Fig. 6A, white box, enlargement in the lower middle and right panel). Some of these mitochondrial structural rearrangements suggest that NE first promoted mitochondrial fusion, perhaps deployed as a defense mechanism for the maintenance of bioenergetics in the presence of NE, but after 72 h NE induced mitochondrial fragmentation, according to the energy impairment observed in Fig. 5 J, K. Immunoblot analysis of proteins involved in mitochondrial dynamics showed a time-dependent significant reduction in the

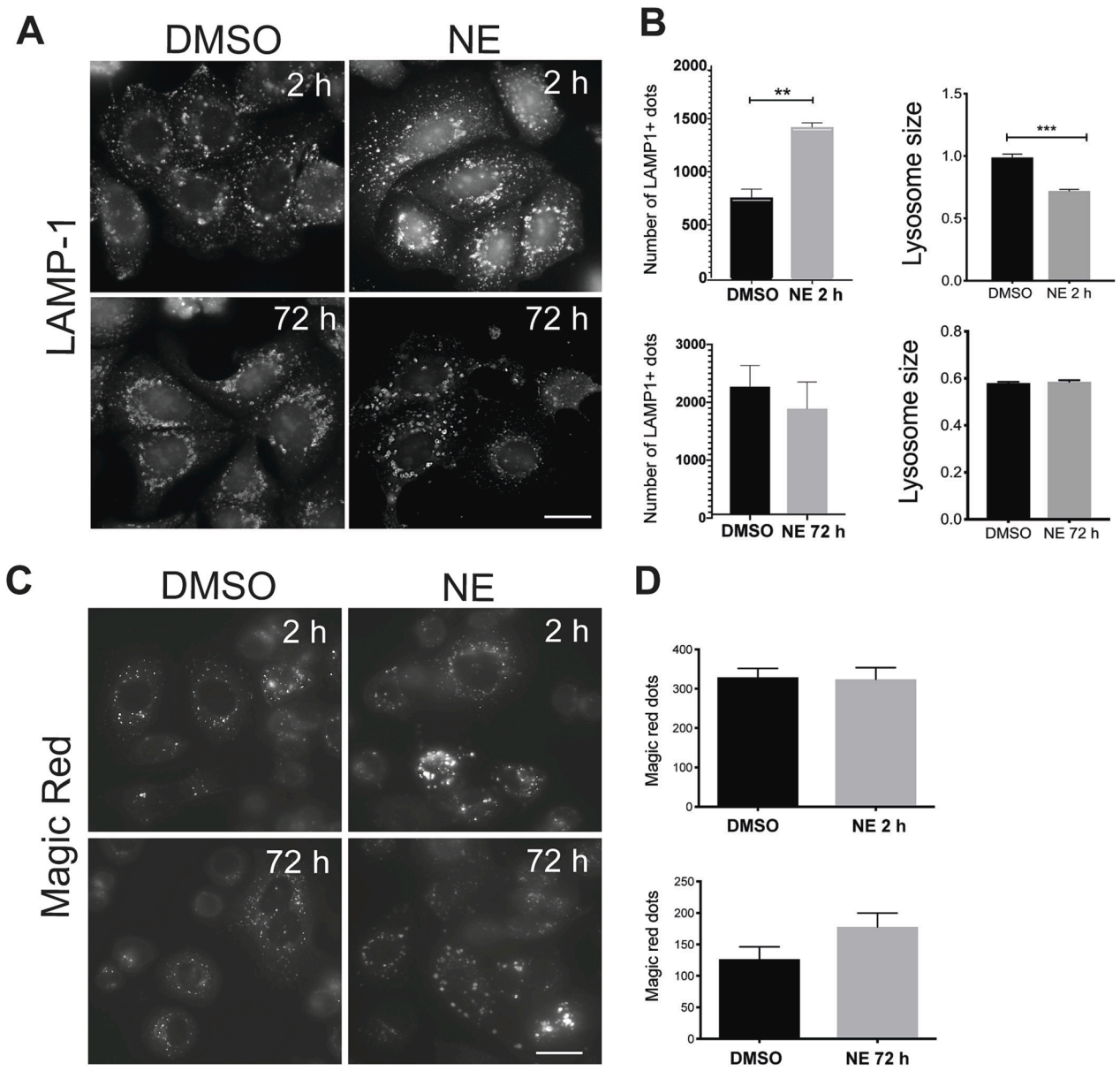

Fig. 3. *NE does not affect lysosomal activity.* (A). Immunofluorescence analysis for the lysosomal membrane protein LAMP-1 in SKBR-3 cells treated with DMSO or 6 nM NE for 2 and 72 h. (B). Graphs showing quantification analysis of LAMP-1 dots number and size in NE- versus DMSO-treated cells (2 and 72 h). Data are expressed as mean ± SEM from three independent experiments in which 50 cells were analyzed for each condition. Unpaired *t*-test. (C). Magic Red (MR) cathepsin B assay shows that NE does not impair lysosomal activity. (D) Graphs showing quantification analysis of MR dots number in NE- versus DMSO-treated cells (2 and 72 h). Data are expressed as mean ± SEM from three independent experiments in which 50 cells were analyzed for each condition. Scale bars: 10 μm. Statistical significance: **p < 0.01, *** p < 0.001.

expression levels of fission-promoting proteins (MFF, DRP-1, and MTFR1) after 2 h of NE treatment [30,31]. By contrast, the levels of the fusion-promoting protein MFN-1 was not affected at 2 h and slightly increased after 72 h of NE treatment (Fig. 6 D) [28]. Collectively, these results indicate that NE unbalances cellular bioenergetics and mitochondrial dynamics, possibly through TFEB modulation.

4. Discussion

ERBB2 + BCa represents an aggressive subtype found in up to 30% of patients. The development of targeted therapies aimed at ERBB2 has dramatically improved the prognosis of patients with ERBB2^{+} BCa. However, primary or acquired resistance to ERBB2-targeted therapies still occurs in some patients because of *ERBB2* mutation or aberrant activation of downstream pathways of ERBB2. Thus, further understanding of how targeted therapies affects cellular pathways that regulate ERBB2 in BCa cells will potentially yield new targeted and/or combinatorial therapies for ERBB2-E BCa. NE is a third-generation pan-ERBB inhibitor approved for ERBB2 + BCa after TZ adjuvant therapy. However, its mechanisms of action at the cellular level are poorly studied [32]. NE exhibits the greatest activity in ERBB2-amplified BCa models and HER2/ERBB2-mutant and EGFR-mutant cells. A recent study demonstrated that sub-micromolar doses of NE inhibit the catalytic activity of ERBB1/2/4, leading to their rapid internalization and proteolytic degradation [15]. Nonetheless, NE also equally targets and inhibits multiple Ste20 family kinases [33] and synergize with the PARP1 inhibitor niraparib to induce DNA damage and cell death [17].

This study dissected the effects of NE, as a single agent, on a panel of phosphoproteins, on autophagy and mitochondrial bioenergetics in the widely used ERBB2 + BCa cell line SKBR3. By phosphokinome array, we

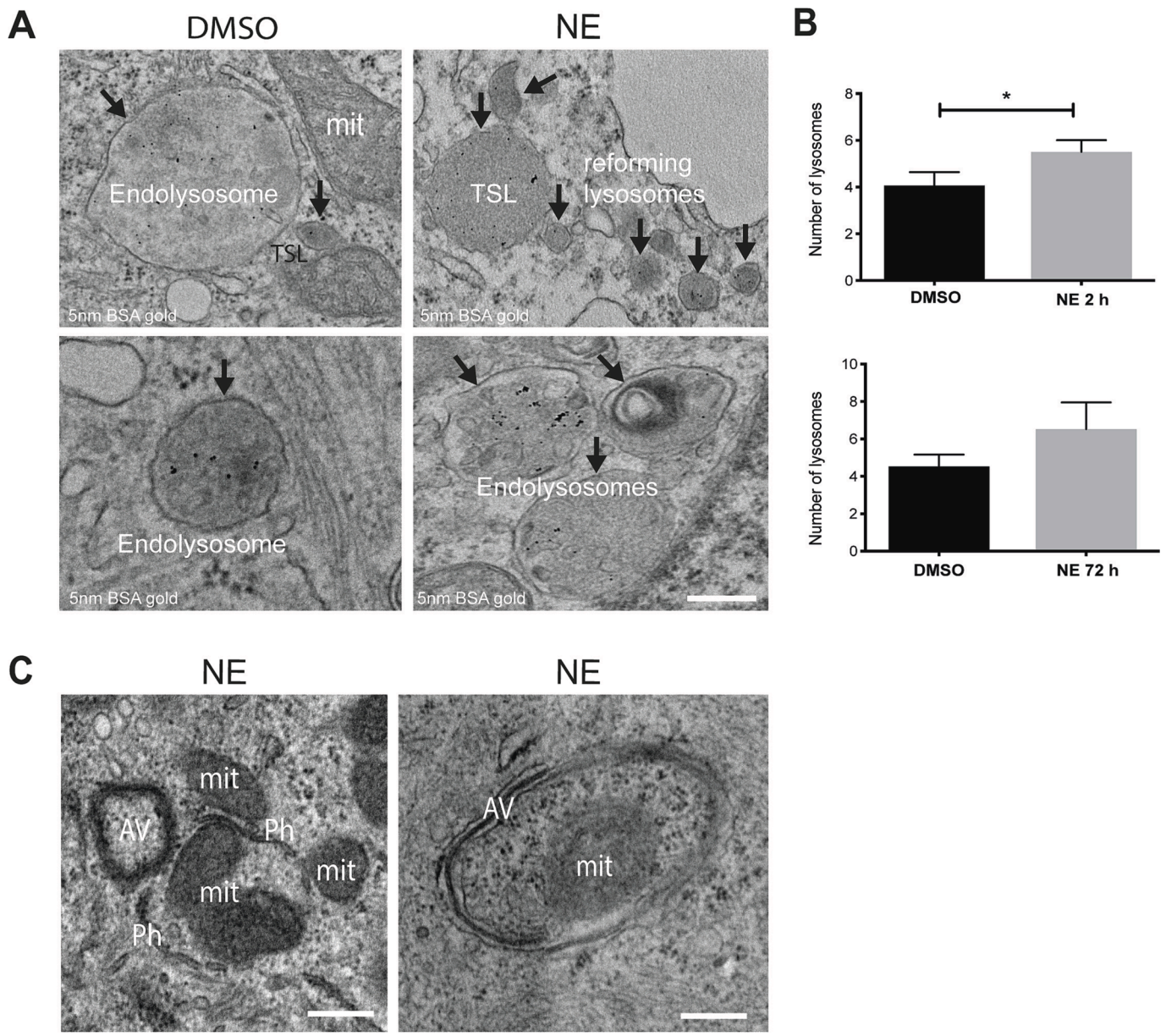

Fig. 4. *Ultrastructural analysis of lysosomal compartment under NE.* (A). Representative EM micrographs of lysosomes probed with 5 nm BSA-gold for 2 h at 37C used as endocytic tracer in SKBR-3 cells treated with 6 nM NE for 2 h (upper panel) and 72 h (bottom panel). Round lysosomes-like organelles heterogenous in size and intraluminal dense content (black arrows). (B). EM morphometry showing increase of lysosomal structures upon 2 h NE. Scale bar: 500 nm. N = 3 independent experiments, 10 whole cells scored for each experiment. (C). Presence of mitophagy in SKBR-3 cells (left image, 2 h NE; right image 72 h NE). TSL: Terminal storage lysosomes, Ph: phagofore membranes, mit: mitochondrion, AV: autophagic vacuole. Scale bars: 1 μm. Statistical significance: *$p < 0.05$.

found that NE time-dependently regulated two sets of protein kinases. The first set was regulated after 2 h of treatment and included some ERBB2 downstream signaling kinases such as ERK1/2, ATK S473, and AKT substrates (PRAS40 and WNK1). By contrast, at 72 h of NE treatment, while the first set was no longer affected, a second set of kinases involved in DDR were strongly inhibited, i.e., CREB S133, CHK2 T68, RSK ½ S221/S227, p53 S46, S15, GSK 3a/b S9/S21, and GSK 3b S9.

Autophagy is a process by which cells recycle and degrade their own components, which can play a complex role in cancer. In cancer cells, autophagy can have both pro-tumorigenic and anti-tumorigenic effects depending on the context and is strictly regulated by the two transcription factors TFEB (transcription factor EB) and TFE3.

In this study, we show that NE transiently boosts the total levels of TFEB and TFE3 and their nuclear fraction, suggesting a potent autophagy induction. The increased levels and activation of TFEB and TFE3 may be a direct consequence of NE-induced dephosphorylation of ERBB2 along with its downstream signaling kinases ATK and ERK in ERBB2 + BCa cells. It is well established that the active forms of AKT and ERK can directly phosphorylate TFEB at S467 and S211, respectively. This results in cytosolic retention of TFEB [34–37]. Therefore, inhibition of pAKT and pERK by NE may promote the activation of TFEB and its translocation into the nucleus. Interestingly, we observed that the ERBB2 + BT474 breast cancer cell line expresses TFEB/TFE3 differently from SKBR-3, with TFE3 being clearly modulated by NE treatment while TFEB was barely detectable in both treated and control cells. This suggests that the regulation of TFEB and TFE3 expression may depend on the specific cellular context in ERBB2 + breast cancer. Additionally, we found that NE promoted an increase in TFEB in the ERBB2-negative but ERBB1 + MDA-MB-231 triple-negative breast cancer cell line, indicating that NE-mediated TFEB activation may also occur through other ERBB

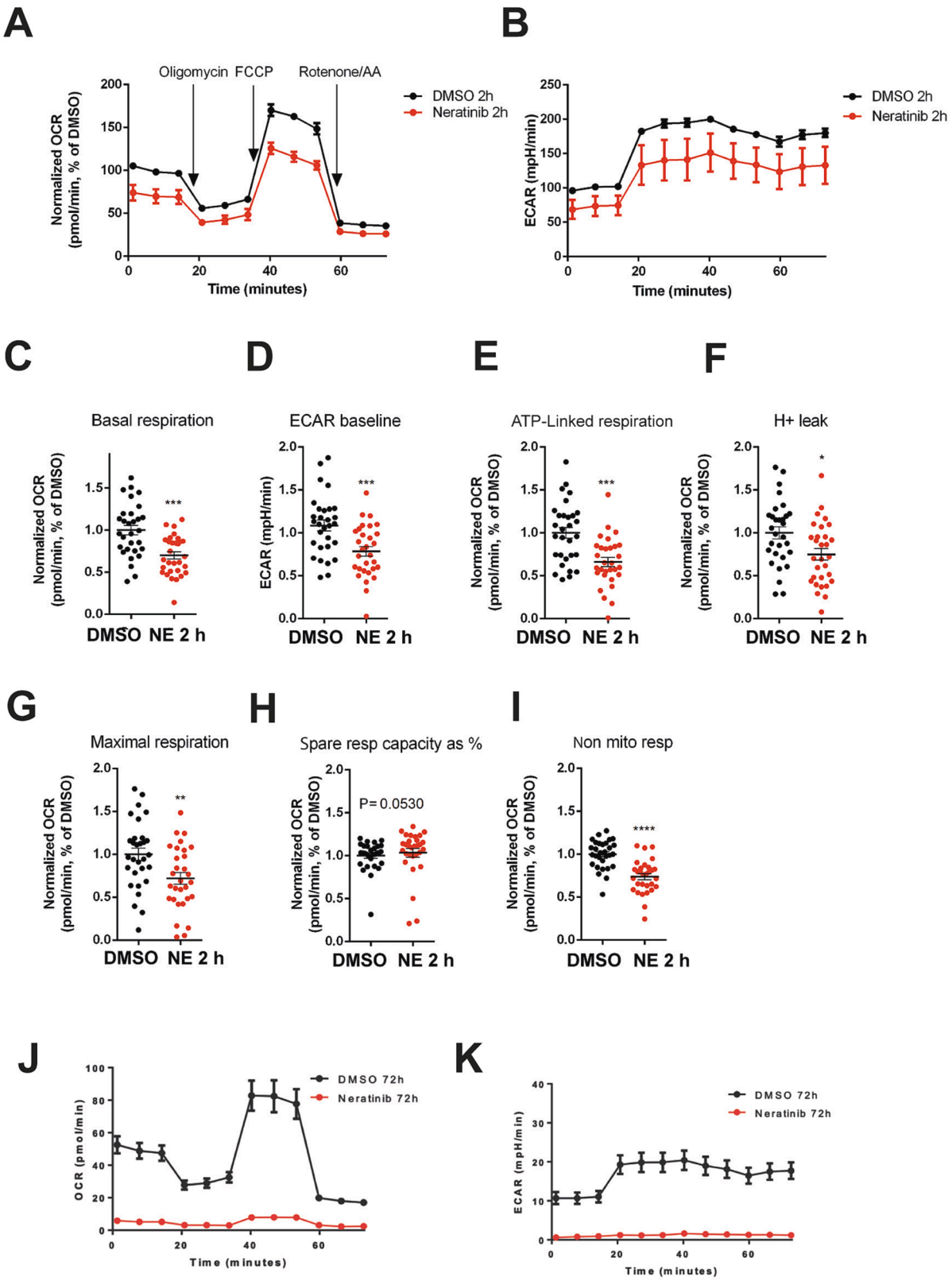

Fig. 5. *NE treatment impairs mitochondrial respiration.* (A). Typical trace from the Seahorse XFp of oxygen consumption rate (OCR) over time (x-axis) measured in DMSO and NE treated SKBR-3 cells. Data represent the mean ± SEM of three independent experiments, 30 replicates/condition. (B). Trace from the Seahorse XFp of extracellular acidification rate (ECAR) over time (x-axis) measured on DMSO and NE treated SKBR-3 cells. (C). Scatter dot plot (line to mean+/- SD) showing basal respiration and (D) ECAR baseline, (E) ATP-linked respiration, (F) H^+ leak, (G) Maximal respiration, (H) spare respiration capacity, (I) non mitochondrial respiration. N = 3 independent experiments, 30 replicates/condition. (J, K) Typical trace from the Seahorse XFp of oxygen consumption rate (OCR) over time (x-axis) and extracellular acidification rate (ECAR) over time (x-axis) measured on DMSO and NE after 72 h (30 replicates). Statistical significance: *$p < 0.05$, **$p < 0.01$, ***$p < 0.001$, ****$p < 0.0001$.

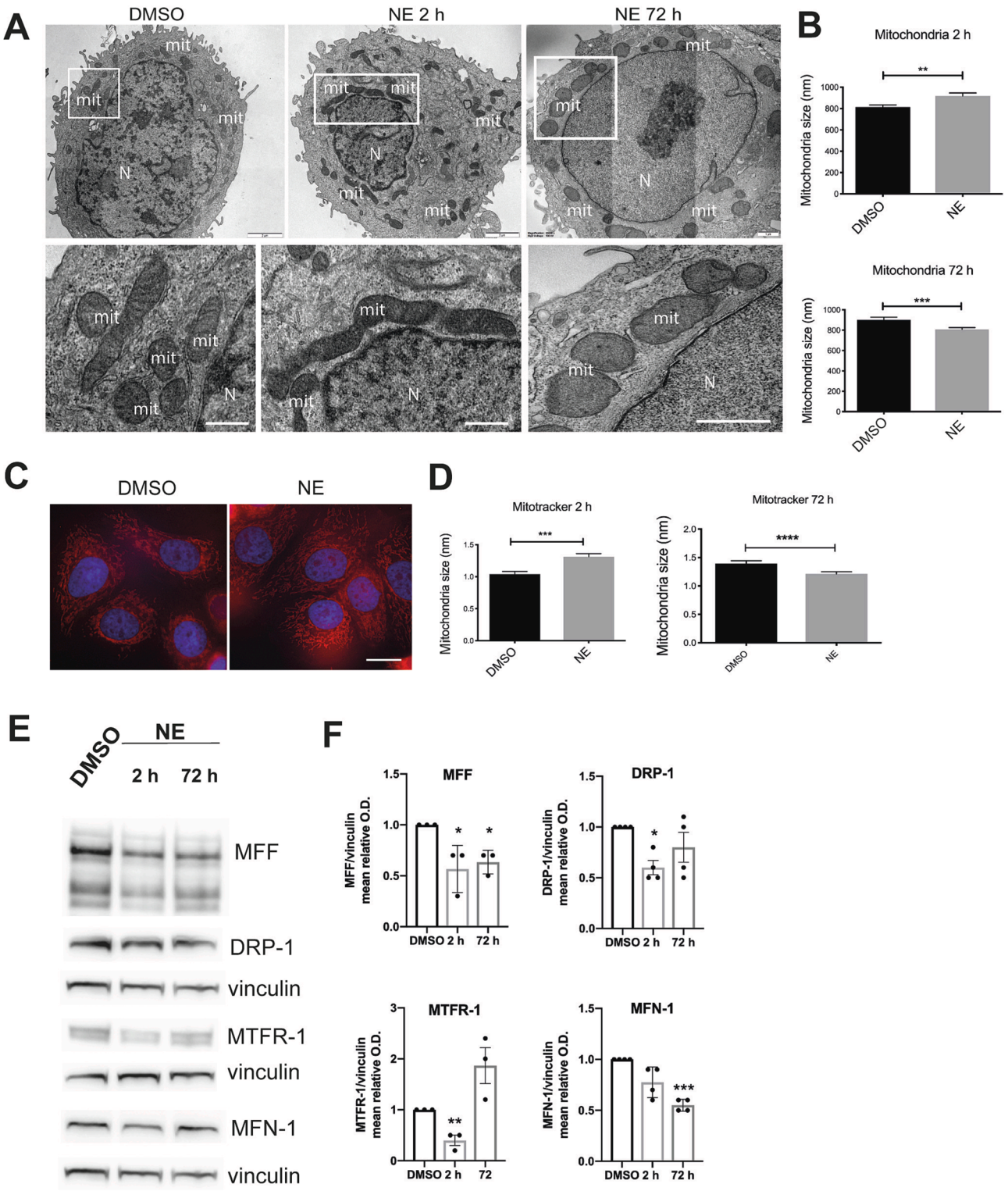

Fig. 6. *NE affects mitochondrial dynamics and morphology.* (A). Electron microscopy images of SKBR-3 cells DMSO and NE treated for 2 and 72 h showing the mitochondrial network (upper images). White boxes identify a small group of mitochondria showed in the lower panel as enlargements. Details of mitochondria morphology in DMSO and 2–72 h NE treated cells. Note that mitochondria appear more electron dense and with less defined cristae in NE treated cells. N: nucleus, mit: mitochondria (B). Quantification of mitochondria long axis by EM morphometry. Mitochondria were measured in 30 whole cells for each experimental condition (n = 3 independent experiments) and plotted as histograms (mean +/-SEM) and significance was determined using Mann-Whitney test). (C). Immunoblot analysis of proteins involved in mitochondrial dynamics revealed downregulation of mitochondrial fission proteins (MFF, DRP1 and MTFR1), while the fusion protein MFN1 was partially up-regulated. Vinculin was used as loading control. (D) The bar graphs represent the mean relative optical density quantification of MFF, DRP-1, MTFR-1 and MFN-1 detected by WB. Values are normalized to DMSO. Error bar = SEM. Significance was determined using one-way ANOVA from n = 3 independent experiments. Statistical significance: *p < 0.05, **p < 0.01, ***p < 0.0001.

receptors besides ERBB2. Finally, we cannot exclude the possibility that other kinases targeted by NE may also contribute to the activation of TFEB and TFE3. For example, an extensive cross-talk between the p53 and TFE3/TFEB pathways has been also associated to the response to DNA damage (DDR) [38]. By phospho-Kinase array analysis, we observed that upon 2 h of NE p53 was hyperphosphorylated in S15, which has a critical role in transactivating p53 responsive promoters [39], suggesting an additional mechanism that may activate TFE3/TFEB. However, further investigations are needed to elucidate the specific molecular mechanisms and signaling pathways involved in the cross-talk between NE, ERBB signaling, and p53 in the regulation of TFEB and TFE3. Following TFEB and TFE3 nuclear translocation, autophagy markers such as LC3I/II and p62/SQSM1 were strongly reduced, demonstrating an active autophagic flux that consumes these proteins. Increased autophagic flux also rapidly depletes the pool of lysosomes in the cell that must be restored to maintain homeostasis. At the ultrastructural level, NE induced an increase in endolysosomes/autolysosomes and dense-core TSLs. These latter are non-acidic and non-hydrolytic lysosomes, which represent reforming lysosomes originating from the tubulation of endolysosomes and/or autolysosomes [40]. A recent study demonstrated that autophagy blockade by gene deletion limits ERBB2 + BCa tumorigenesis by perturbing ERBB2 trafficking and promoting release through small extracellular vesicles [24]. These results agree with the findings of our previous work that low nanomolar doses of NE potentiated clathrin-mediated endocytic pathways, multivesicular body formation, and extracellular vesicles release without downregulating ERBB2 [9]. Moreover, recent evidence shows that MQC, including maintenance of the quantity, morphology, and function of mitochondria, is controlled by TFEB, and TFE3 [28]. In this study, NE strongly time-dependently affects mitochondrial dynamics, morphology, and function and TFEB/TFE3 levels/localization and activity. Specifically, our ultrastructural analysis revealed time-dependent mitochondrial fusion/fission events and cristae rearrangements, whereas metabolic analysis by Seahorse confirmed a significant decrease in ATP production, OCR, and ECAR rates already after 2 h of NE treatment. We might speculate that NE affects MQC by modulation TFEB and TFE3 levels, localization, or activation status. The effect of NE specifically on clathrin-mediated endocytosis appears to be an ERBB2-dependent process [9,12], whereas the effects on autophagy and MQC appear to be more generally ERBB-dependent and driven through TFEB and TFE3, rather than ERBB2-specific [41]. Concerning the inhibition of cell survival caused by NE in our model system, it may result from the combined effect of several processes such as cell cycle arrest, apoptosis induction, enhanced autophagy, and inhibition of mitochondrial metabolism.

To the best of our knowledge, this study reports the first evidence describing NE as an activator/agonist of TFEB and TFE3 transcription factors. Additionally, NE modulates the phosphorylation status of downstream kinases specific to ERBB2, thereby regulating cell survival as well as kinases involved in DNA damage repair. Notably, T-DXd, an approved antibody-drug conjugate for heavily pretreated patients with ERBB2 + BCa, promotes DNA damage by targeting topoisomerase 1 [41]. Since NE demonstrates effectiveness in activating autophagy and inhibiting DDR proteins, while T-DXd induces DNA damage through the release of DXd from lysosomes, further investigations are warranted to explore potential combinatorial therapies. The findings of this study collectively demonstrate that NE disrupts crucial cellular processes associated with cell survival and metabolic adaptation, which are also implicated in the development of therapeutic resistance. Consequently, additional studies are necessary to evaluate whether stimulating autophagy via targeting TFEB and/or TFE3 could serve as an additional strategy that synergizes with current anti-ERBB2 agents.

CRediT authorship contribution statement

Grazia Bellese: Investigation, Validation. **Erica Tagliatti:** Investigation, Validation. **Maria Cristina Gagliani:** Investigation, Validation. **Sara Santamaria:** Investigation, Validation. **Pietro Arnaldi:** Investigation, Validation. **Paola Falletta:** Supervision. **Paola Rusmini:** Investigation, Validation. **Michela Matteoli:** Supervision. **Patrizio Castagnola:** Conceptualization, Writing – review & editing, Funding acquisition, Supervision. **Katia Cortese:** Conceptualization, Writing – review & editing, Funding acquisition, Supervision.

Declaration of Competing Interest

The authors declare that they have no known competing financial interests or personal relationships that could have appeared to influence the work reported in this paper.

Data availability

Data will be made available on request.

Acknowledgements

We thank the University of Genoa for funding the acquisition of the HITACHI 120 kV TEM microscope HT7800, (Grant D.R. 3404, Heavy Equipment). We thank Valeria Crippa and Veronica Ferrari (University of Milan) for helpful discussions and Genni Desiato (Humanitas) for assistance with Seahorse experiments. The authors would like to thank Enago (www.enago.com) for the English language review. The author(s) disclosed receipt of the following financial support for the research, authorship, and/or publication of this article: this work was supported by grants from Italian Ministry of Health (Ricerca Corrente) to PC and by University of Genova research grant funding (Fondi Ricerca Ateneo, 100008-2022-KC-FRA_ANATOMIA), and by MUR (Ministero dell'Università e della Ricerca) PRIN2020PBS5MJ to KC.

Ethics approval and consent to participate

Non applicable.

Consent for publication

Not applicable.

Availability of data and material

The data supporting the conclusions of this article are included within the article and its additional files.

References

[1] Y. Yarden, M.X. Sliwkowski, Untangling the ErbB signalling network, Epub ahead of print, Nat. Rev. Mol. Cell Biol. 2 (2) (2001) 127–137.
[2] N.E. Hynes, G. MacDonald, ErbB receptors and signaling pathways in cancer, Curr. Opin. Cell Biol. 21 (2) (2009) 177–184.
[3] P. Castagnola, G. Bellese, F. Birocchi, M.C. Gagliani, C. Tacchetti, K. Cortese, Identification of an HSP90 modulated multi-step process for ERBB2 degradation in breast cancer cells, Oncotarget 7 (51) (2016) 85411–85429.
[4] E. Tagliatti, K. Cortese, Imaging Endocytosis Dynamics in Health and Disease, Membranes 12 (2022), https://doi.org/10.3390/membranes12040393.
[5] P. Bagnato, A. Castagnino, K. Cortese, M. Bono, S. Grasso, G. Bellese, T. Daniele, R. Lundmark, P. Defilippi, P. Castagnola, C. Tacchetti, Cooperative but distinct early co-signaling events originate from ERBB2 and ERBB1 receptors upon trastuzumab treatment in breast cancer cells, Oncotarget 8 (36) (2017) 60109–60122.
[6] C. D'Alesio, G. Bellese, M.C. Gagliani, A. Lechiara, M. Dameri, E. Grasselli, L. Lanfrancone, K. Cortese, P. Castagnola, The chromodomain helicase CHD4 regulates ERBB2 signaling pathway and autophagy in ERBB2+ breast cancer cells, Biol. Open 8 (2019) 1–8.
[7] I. Mellman, Y. Yarden, Endocytosis and cancer, Epub ahead of print, Cold Spring Harb. Perspect. Biol. 55 (12) (2013) a016949–a.
[8] D. Harari, Y. Yarden, Molecular mechanisms underlying ErbB2/HER2 action in breast cancer, Epub ahead of print, Oncogene 19 (53) (2000) 6102–6114.

[9] S. Santamaria, M.C. Gagliani, G. Bellese, S. Marconi, A. Lechiara, M. Dameri, C. Aiello, E. Tagliatti, P. Castagnola, K. Cortese, Imaging of Endocytic Trafficking and Extracellular Vesicles Released Under Neratinib Treatment in ERBB2+ Breast Cancer Cells, J. Histochem. Cytochem. 69 (7) (2021) 461–473.
[10] J. Cortés, S.-B. Kim, W.-P. Chung, S.-A. Im, Y.H. Park, R. Hegg, M.H. Kim, L.-M. Tseng, V. Petry, C.-F. Chung, H. Iwata, E. Hamilton, G. Curigliano, B. Xu, C.-S. Huang, J.H. Kim, J.W.Y. Chiu, J.L. Pedrini, C. Lee, Y. Liu, J. Cathcart, E. Bako, S. Verma, S.A. Hurvitz, Trastuzumab Deruxtecan versus Trastuzumab Emtansine for Breast Cancer, N. Engl. J. Med. 386 (12) (2022) 1143–1154.
[11] Y. Ogitani, T. Aida, K. Hagihara, J. Yamaguchi, C. Ishii, N. Harada, M. Soma, H. Okamoto, M. Oitate, S. Arakawa, T. Hirai, R. Atsumi, T. Nakada, I. Hayakawa, Y. Abe, T. Agatsuma, DS-8201a, a novel HER2-targeting ADC with a novel DNA topoisomerase I inhibitor, demonstrates a promising antitumor efficacy with differentiation from T-DM1, Clin. Cancer Res. 22 (20) (2016) 5097–5108.
[12] K. Cortese, M.T. Howes, R. Lundmark, E. Tagliatti, P. Bagnato, A. Petrelli, M. Bono, H.T. McMahon, R.G. Parton, C. Tacchetti, The HSP90 inhibitor geldanamycin perturbs endosomal structure and drives recycling ErbB2 and transferrin to modified MVBs/lysosomal compartments, Epub ahead of print, Mol. Biol. Cell. 24 (2) (2013) 129–144.
[13] A. Chan, B. Moy, J. Mansi, B. Ejlertsen, F.A. Holmes, S. Chia, H. Iwata, M. Gnant, S. Loibl, C.H. Barrios, I. Somali, S. Smichkoska, N. Martinez, M.G. Alonso, J.S. Link, I.A. Mayer, S. Cold, S.M. Murillo, F. Senecal, K. Inoue, M. Ruiz-Borrego, R. Hui, N. Denduluri, D. Patt, H.S. Rugo, S.R.D. Johnston, R. Bryce, B.o. Zhang, F. Xu, A. Wong, M. Martin, Final Efficacy Results of Neratinib in HER2-positive Hormone Receptor-positive Early-stage Breast Cancer From the Phase III ExteNET Trial, Clin. Breast Cancer 21 (1) (2021) 80–91.e7.
[14] A. Chan, S. Delaloge, F.A. Holmes, B. Moy, H. Iwata, V.J. Harvey, N.J. Robert, T. Silovski, E. Gokmen, G. von Minckwitz, B. Ejlertsen, S.K.L. Chia, J. Mansi, C. H. Barrios, M. Gnant, M. Buyse, I. Gore, J. Smith, G. Harker, N. Masuda, K. Petrakova, A.G. Zotano, N. Iannotti, G. Rodriguez, P. Tassone, A. Wong, R. Bryce, Y. Ye, B. Yao, M. Martin, Neratinib after trastuzumab-based adjuvant therapy in patients with HER2-positive breast cancer (ExteNET): A multicentre, randomised, double-blind, placebo-controlled, phase 3 trial, Epub ahead of print, Lancet Oncol. 17 (3) (2016) 367–377.
[15] Y. Zhang, J. Zhang, C. Liu, S. Du, L.u. Feng, X. Luan, Y. Zhang, Y. Shi, T. Wang, Y. Wu, W. Cheng, S. Meng, M. Li, H. Liu, Neratinib induces ErbB2 ubiquitylation and endocytic degradation via HSP90 dissociation in breast cancer cells, Epub ahead of print, Cancer Lett. 382 (2) (2016) 176–185.
[16] L. Booth, J.L. Roberts, P. Samuel, F. Avogadri-Connors, R.E. Cutler, A.S. Lalani, A. Poklepovic, P. Dent, The irreversible ERBB1/2/4 inhibitor neratinib interacts with the PARP1 inhibitor niraparib to kill ovarian cancer cells, Cancer Biol. Ther. 19 (6) (2018) 525–533.
[17] P. Dent, L. Booth, J.L. Roberts, J. Liu, A. Poklepovic, A.S. Lalani, D. Tuveson, J. Martinez, J.F. Hancock, Neratinib inhibits Hippo/YAP signaling, reduces mutant K-RAS expression, and kills pancreatic and blood cancer cells, Epub ahead of print, Oncogene 38 (30) (2019) 5890–5904.
[18] D.M. Collins, N.T. Conlon, S. Kannan, C.S. Verma, L.D. Eli, A.S. Lalani, J. Crown, Preclinical characteristics of the irreversible pan- her kinase inhibitor neratinib compared with lapatinib: Implications for the treatment of HER2- positive and HER2-mutated breast cancer, Cancers (Basel) 11 (6) (2019) 737.
[19] K. Aljakouch, T. Lechtonen, H.K. Yosef, M.K. Hammoud, W. Alsaidi, C. Kötting, C. Mügge, R. Kourist, S.F. El-Mashtoly, K. Gerwert, Raman Microspectroscopic Evidence for the Metabolism of a Tyrosine Kinase Inhibitor, Neratinib, in Cancer Cells, Angewandte Chemie - International Edition 57 (24) (2018) 7250–7254.
[20] P. Dent, L. Booth, J.L. Roberts, A. Poklepovic, D. Cridebring, E.M. Reiman, Inhibition of heat shock proteins increases autophagosome formation, and reduces the expression of APP, Tau, SOD1 G93A and TDP-43, Aging 13 (13) (2021) 17097–17117.
[21] A.V. Onorati, M. Dyczynski, R. Ojha, R.K. Amaravadi, Targeting autophagy in cancer, Cancer 124 (16) (2018) 3307–3318.
[22] X. Zeng, H. Zhao, Y. Li, J. Fan, Y. Sun, S. Wang, Z. Wang, P. Song, D. Ju, Targeting Hedgehog signaling pathway and autophagy overcomes drug resistance of BCR-ABLpositive chronic myeloid leukemia, Autophagy 11 (2) (2015) 355–372.
[23] X. Zhu, L. Wu, H. Qiao, T. Han, S. Chen, X. Liu, R.u. Jiang, Y. Wei, D. Feng, Y. Zhang, Y. Ma, S. Zhang, J. Zhang, Autophagy Stimulates Apoptosis in HER2-Overexpressing Breast Cancers Treated by Lapatinib, J. Cell. Biochem. 114 (12) (2013) 2643–2653.
[24] M. Hao, S.K. Yeo, J.-L. Guan, Autophagy inhibition perturbs ERBB2 trafficking and abolishes tumorigenesis in ERBB2-driven breast cancer, Autophagy 17 (4) (2021) 1059–1060.
[25] P. Rusmini, K. Cortese, V. Crippa, R. Cristofani, M.E. Cicardi, V. Ferrari, G. Vezzoli, B. Tedesco, M. Meroni, E. Messi, M. Piccolella, M. Galbiati, M. Garrè, E. Morelli, T. Vaccari, A. Poletti, Trehalose induces autophagy via lysosomal-mediated TFEB activation in models of motoneuron degeneration, Epub ahead of print, Autophagy 15 (4) (2019) 631–651.
[26] L. Booth, J.L. Roberts, A. Poklepovic, J. Kirkwood, C. Sander, F. Avogadri-Connors, R.E. Cutler Jr, A.S. Lalani, P. Dent, The levels of mutant K-RAS and mutant N-RAS are rapidly reduced in a Beclin1 / ATG5 -dependent fashion by the irreversible ERBB1/2/4 inhibitor neratinib, Cancer Biol. Ther. 19 (2) (2018) 132–137.
[27] C. Settembre, R. Zoncu, D.L. Medina, F. Vetrini, S. Erdin, T. Huynh, M. Ferron, G. Karsenty, M.C. Vellard, V. Facchinetti, D.M. Sabatini, A. Ballabio, A lysosome-to-nucleus signalling mechanism senses and regulates the lysosome via mTOR and TFEB, EMBO J. 31 (5) (2012) 1095–1108.
[28] S. Wang, Y. Chen, X. Li, W. Zhang, Z. Liu, M. Wu, Q. Pan, H. Liu, Emerging role of transcription factor EB in mitochondrial quality control, Biomed. Pharmacother. 128 (2020).
[29] Bright NA, Reaves BJ, Mullock BM, et al. Dense core lysosomes can fuse with late endosomes and are re-formed from the resultant hybrid organelles. J. Cell Sci.
[30] M. Monticone, I. Panfoli, S. Ravera, R. Puglisi, M.-M. Jiang, R. Morello, S. Candiani, L. Tonachini, R. Biticchi, A. Fabiano, R. Cancedda, C. Boitani, P. Castagnola, The nuclear genes Mtfr1 and Dufd1 regulate mitochondrial dynamic and cellular respiration, J. Cell. Physiol. 225 (3) (2010) 767–776.
[31] M. Monticone, L. Tonachini, S. Tavella, P. Degan, R. Biticchi, F. Palombi, R. Puglisi, C. Boitani, R. Cancedda, P. Castagnola, Impaired expression of genes coding for reactive oxygen species scavenging enzymes in testes of Mtfr1/Chppr-deficient mice, Reproduction 134 (3) (2007) 483–492.
[32] A. Canonici, M. Gijsen, M. Mullooly, R. Bennett, N. Bouguern, K. Pedersen, N. A. O'Brien, I. Roxanis, J.-L. Li, E. Bridge, R. Finn, D. Slamon, P. McGowan, M. J. Duffy, N. O'Donovan, J. Crown, A. Kong, Neratinib overcomes trastuzumab resistance in HER2 amplified breast cancer, Epub ahead of print, Oncotarget 4 (10) (2013) 1592–1605.
[33] L. Booth, A. Poklepovic, P. Dent, Not the comfy chair! Cancer drugs that act against multiple active sites, Expert Opin. Ther. Targets 23 (11) (2019) 893–901.
[34] Palmieri M, Pal R, Nelvagal HR, et al. MTORC1-independent TFEB activation via Akt inhibition promotes cellular clearance in neurodegenerative storage diseases. Nat. Commun; 8. Epub ahead of print 2017. DOI: 10.1038/ncomms14338.
[35] M. Chen, Y. Dai, S. Liu, Y. Fan, Z. Ding, D. Li, Tfeb biology and agonists at a glance, Cells 10 (2) (2021) 333.
[36] J. Wang, M.W. Whiteman, H. Lian, G. Wang, A. Singh, D. Huang, T. Denmark, A non-canonical MEK/ERK signaling pathway regulates autophagy via regulating Beclin 1, J. Biol. Chem. 284 (32) (2009) 21412–21424.
[37] M. Palmieri, R. Pal, M. Sardiello, AKT modulates the autophagy-lysosome pathway via TFEB, Cell Cycle 16 (13) (2017) 1237–1238.
[38] Brady OA, Jeong E, Martina JA, et al. The transcription factors TFE3 and TFEB amplify p53 dependent transcriptional programs in response to DNA damage. *Elife*; 7. Epub ahead of print 6 December 2018. DOI: 10.7554/eLife.40856.
[39] J. Loughery, M. Cox, L.M. Smith, D.W. Meek, Critical role for p53-serine 15 phosphorylation in stimulating transactivation at p53-responsive promoters, Nucleic Acids Res. 42 (12) (2014) 7666–7680.
[40] N. Bright, L. Davis, J.P. Luzio, Endolysosomes Are the Principal Intracellular Sites of Acid Hydrolase Activity, Epub ahead of print, Curr. Biol. 26 (17) (2016) 2233–2245.
[41] Indini A, Rijavec E, Grossi F. Molecular Sciences Trastuzumab Deruxtecan: Changing the Destiny of HER2 Expressing Solid Tumors. Epub ahead of print 2021. DOI: 10.3390/ijms22094774.